AD-A170 800 MECHANISTIC UNDERSTANDING OF POWDER COMPACTION IN METALS(U) CORNELL UNIV ITHACA NY DEPT OF MATERIALS SCIENCE AND ENGINEERING R RAJ 06 MAR 86 1/1

UNCLASSIFIED AFOSR-TR-86-0505 AFOSR-84-0133 F/G 11/6 NL

END
DATE FILMED
9-86

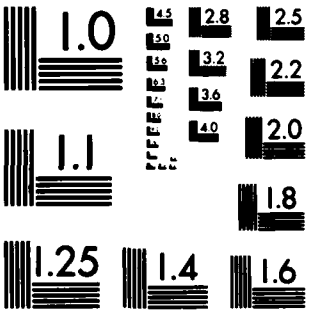

MICROCOPY RESOLUTION TEST CHART
NATIONAL BUREAU OF STANDARDS-1963-A

AD-A170 800

DTIC FILE COPY

(2)

SECURITY CLASSIFICATION OF THIS PAGE

DTIC ELECTE AUG 13 1986 S D

REPORT DOCUMENTATION PAGE

1a. REPORT SECURITY CLASSIFICATION	1b. RESTRICTIVE MARKINGS
2a. SECURITY CLASSIFICATION AUTHORITY	3. DISTRIBUTION/AVAILABILITY OF REPORT: DISTRIBUTION STATEMENT A Approved for public release; Distribution Unlimited
2b. DECLASSIFICATION/DOWNGRADING SCHEDULE D	
4. PERFORMING ORGANIZATION REPORT NUMBER(S): First Annual Technical Report	5. MONITORING ORGANIZATION REPORT NUMBER(S): AFOSR-TR- 86-0505
6a. NAME OF PERFORMING ORGANIZATION: Cornell University	6b. OFFICE SYMBOL (If applicable):
7a. NAME OF MONITORING ORGANIZATION: AFOSR Attn: Dr. A. H. Rosenstein	
6c. ADDRESS (City, State and ZIP Code): Dept. Materials Science & Engineering Ithaca, NY 14853-1501	7b. ADDRESS (City, State and ZIP Code): Bldg. 410 Bolling Air Force Base Washington, DC 20332
8a. NAME OF FUNDING/SPONSORING ORGANIZATION: AFOSR	8b. OFFICE SYMBOL (If applicable): NE
9. PROCUREMENT INSTRUMENT IDENTIFICATION NUMBER: AFOSR-84-0133	
8c. ADDRESS (City, State and ZIP Code): see 7b	10. SOURCE OF FUNDING NOS.

PROGRAM ELEMENT NO.	PROJECT NO.	TASK NO.	WORK UNIT NO.
	2306	A1	

11. TITLE (Include Security Classification): Mechanisms of Powder Compaction of Metals

12. PERSONAL AUTHOR(S): Professor Rishi Raj, Principal Investigator

13a. TYPE OF REPORT	13b. TIME COVERED	14. DATE OF REPORT (Yr., Mo., Day)	15. PAGE COUNT
Annual Technical Report	FROM 4/1/84 TO 2/15/86	1986, 03, 06	35

16. SUPPLEMENTARY NOTATION

17. COSATI CODES			18. SUBJECT TERMS (Continue on reverse if necessary and identify by block number)
FIELD	GROUP	SUB. GR.	

19. ABSTRACT (Continue on reverse if necessary and identify by block number) In this, the first annual report, results from hot-pressing experiments on $Ni_xAl_{(1-x)}$ powders are described. The stoichiometry of the alloy is varied in the range $0.64<x<0.52$. The change in composition allows us to change the diffusion coefficient by nearly two orders of magnitude. The principal mechanisms of powder compaction are plastic flow (by dislocations) and diffusional teansport. The relative contribution of these two mechanisms can, therefore, be separated by varying the composition. Also, the dislocation mechanism is expected to dominate when densification is carried out at high stresses. Dislocation activity is also expected to influence microstructure evolution by dynamic recrystallization. The results described in this report demonstrate that the diffusional and dislocation mechanisms can indeed be separated by changing the stress and the composition. At high stresses, we have found evidence of precipitation of new grains at interfaces. Current and future work is being directed toward understanding the role of shear strain in densification and in microstructure evolution during powder compaction.

20. DISTRIBUTION/AVAILABILITY OF ABSTRACT	21. ABSTRACT SECURITY CLASSIFICATION
UNCLASSIFIED/UNLIMITED ☐ SAME AS RPT. ☐ DTIC USERS ☐	

22a. NAME OF RESPONSIBLE INDIVIDUAL	22b. TELEPHONE NUMBER (Include Area Code)	22c. OFFICE SYMBOL
Dr Rosenstein	202-767-4933	AFOSR/NE

DD FORM 1473, 83 APR EDITION OF 1 JAN 73 IS OBSOLETE.

SECURITY CLASSIFICATION OF THIS PAGE

AFOSR-TR- 86-0505

ANNUAL TECHNICAL REPORT

(4/1/84 - 2/15/86)

MECHANISTIC UNDERSTANDING OF POWDER COMPACTION IN METALS

AFOSR-84-0133

Prepared for:

Air Force Office of Scientific Research
410 Bolling Air Force Base
Solid State Division
Washington, DC 22209
Attn: Dr. A.H. Rosenstein

Prepared by:

Professor Rishi Raj
Department of Materials Science and Engineering
Cornell University
Ithaca, NY 14853-1501

February 1986

Approved for public release,
distribution unlimited

ABSTRACT

In this, the first annual report, results from hot-pressing experiments on $Ni_xAl_{(1-x)}$ powders are described. The stoichiometry of the alloy is varied in the range $0.64<x<0.52$. The change in composition allows us to change the diffusion coefficient by nearly two orders of magnitude. The principal mechanisms of powder compaction are plastic flow (by dislocations) and diffusional transport. The relative contribution of these two mechanisms can, therefore, be separated by varying the composition. Also, the dislocation mechanism is expected to dominate when densification is carried out at high stresses. Dislocation activity is also expected to influence microstructure evolution by dynamic recrystallization. The results described in this report demonstrate that the diffusional and dislocation mechanisms can indeed be separated by changing the stress and the composition. At high stresses, we have found evidence of precipitation of new grains at interfaces. Current and future work is being directed toward understanding the role of shear strain in densification and in microstructure evolution during powder compaction.

AIR FORCE OFFICE OF SCIENTIFIC RESEARCH (AFSC)
NOTICE OF TRANSMITTAL TO DTIC
This technical report has been reviewed and is approved for public release IAW AFR 190-12.
Distribution is unlimited.
MATTHEW J. KEPPER
Chief, Technical Information Division

86 8 13 082

BACKGROUND

Structural materials for engineering applications nearly always consist of a matrix phase which is dispersed with a second phase of greater hardness. The volume fraction, distribution and the morphology of the second phase, control the vital mechanical properties of the composite. These properties include the modulus, yield strength, ductility and flaw sensitive properties such as fatigue.

The optimum microstructures for structural materials can be obtained via several processing paths. For example, nickel-base superalloys, which may contain upto fifty percent of the gamma prime phase, are processed by precipitating the second phase through heat treatment. Such a process, however, is limited to situations where the constituents of the second phase can be be put into solid solution at high temperatures. Powder metallurgy offers a more versatile method of material fabrication since second phase constituents can be mechanically mixed with the matrix[1], or they can be added to the matrix by rapid quenching[2]. The powders so produced can be then consolidated at elevated temperature. In the case of aluminum alloys, for example, powder metallurgy is the only route for introducing significant volume fractions of chromium, zirconium, and titanium intermetallics to improve creep strength[3]. While such powder processes need further development and understanding, the potential that powder-metallurgy holds for fabricating special materials cannot be disputed.

The recent availability of ceramic fibers and whiskers has raised the possibility of producing metal matrix - ceramic composites. Since the ceramics have a much higher modulus than the metals, these composites can be designed to have a considerably higher specific modulus than that of

QUALITY INSPECTED 1

odes
/or
ial
A-1

simple metals. Again, powder metallurgy is the only viable technique for fabricating such materials. The mechanical properties of metal-ceramic composites are sensitive to the tensile and the shear strength of the metal-ceramic interface. An understanding of the structure property relationship of these interfaces are important not only for the eventual performance of the composite but also for the fabrication process since the rheology of the composites will depend on the bonding between the ceramic and the metal.

Powder compaction at elevated temperatures can be carried out by one or some combination of the following processes: sintering, hot-isostatic-pressing, hot-pressing and sinter-forging. The compaction process aims not only to achieve fully density, but also to impart a precise shape to the part, and to develop a desirable microstructure without introducing defects such as microcracks. The mechanisms of powder compaction may be broadly classified into two classes: those relying on plastic flow by dislocations, and those that are dependent on diffusional transport. The relative contribution of each depends on the pressure-time-temperature cycle used to densify the powder. These concepts have been presented in a map format by Ashby and co-workers[4,5,6]. The maps developed so far, however, have not considered the microstructure evolution aspect of powder compaction. This is important because microstructural changes such as grain growth can reduce the rate of diffusional densification mechansim. Dislocation mechansims, on the other hand, can lead to grain refinement through dynamic recrystallization.

In this report we discuss first the mechanisms of densification. This is followed by a discussion of why nickel-aluminum was chosen as the model material for experiments. Experimental results are then presented which

show a transition from the diffusional to the dislocation mechanism as the stress is increased. Evidence of crystallization of new grains when densification is carried out at high stresses is presented. Finally theoretical interpretation of the experimental results is given.

THEORETICAL CONSIDERATIONS

Mechanisms

The closure of pores in a powder compact may be achieved either by deformation, or by diffusional transport of atoms from the grain interfaces into the pores. The deformation mechanism depends on dislocations and is independent of the grain size. In the case of diffusional transport, however, the diffusion distance is equal to one half of the grain size, and the rate of pore closure, therefore, is sensitive to the grain size. Thus grain growth during the compaction process will affect the relative contribution of the dislocation and the diffusional mechanisms to densification.

An inspection of deformation mechanism maps[7] shows that stress and temperature influence the relative dominance of the dislocation and diffusional mechanisms. For a given temperature the diffusional mechanism dominates at low stresses, but yields to the dislocation mechanism at high stresses. The same phenomenology is expected in the compaction of powders. The distinction between the dominant densification mechanism is important because the development of the microstructure depends on it. The diffusional mechanism may in fact induce grain growth, which, in turn, would depress the rate of densification, effectively leading to an increasing resistance to densification. The dislocation mechanism on the other hand can produce dynamic recrystallization. Recrystallization can be beneficial since it dissolves the prior particle grain boundaries where impurity segregation may be heavy, and replaces them by fresh boundaries. Refinement of the micorstructure can also improve flaw sensitive mechanical properties such as fatigue.

The constitutive equations for densification are related to the constitutive equations for the deformation of fully dense material. The deformation equations for dislocation and diffusional mechanisms have the following form:

$$\dot{\epsilon} = A\sigma^n \qquad (1)$$

and

$$\dot{\epsilon} = \frac{B}{d^3}\sigma \qquad (2).$$

where equation (1) represents dislocation flow and (2) describes diffusional flow. In (1) and (2), $\dot{\epsilon}$ is the shear or the effective strain rate, and σ is the effective stress. A and B are temperature dependent parameters,while the parameter d in equation (2) is the grain size. The parameter n is the power-law exponent; its value is usually greater than 3. Equation (2) is written for the case where matter is transported by grain boundary diffusion; diffusion also occurs through the grain matrix in which case the strain rate varies as the square rather than the third powder of the grain size. Clearly the grain size has a strong influence on the diffusional strain rate. The forms of equations (1) and (2) imply that a larger grain size and a higher stress will increase the rate of dislocation strain rate relative to the diffusional strain rate.

The theoretical derivations for the rate of densification are constructed by defining boundary value problems which pay attention to the geometry of the pore, and to the flow lines along which material is transported to fill the pores. The constitutive equations for densification, therefore, have the same form as equations (1) and (2),

except that the densification rate also depends on the pore volume[6,9,10,11,12]. The general form for the equations for densification rate is as follows:

$$\dot{\rho} = A f(\rho) p^n \qquad (3)$$

and

$$\dot{\rho} = \frac{B}{d^3} g(\rho) p \qquad (4)$$

where equation (3) represents densification by dislocation flow and (4) describes diffusional densification. Here $\dot{\rho}$ is the densification rate and $f(\rho)$ and $g(\rho)$ are functions of the density. The parameter d in (4) is used interchangeably for the powder-particle size or the grain size. The first definition is more appropriate in the early stages of densification when ρ is less than about 80% and the porosity is interconnected, while the grain size is the more appropriate parameter in the final stages of densification. Since the driving force for densification is the hydrostatic pressure instead of the shear stress, note that the deviatoric stress in equations (1) and (2) has been replaced by the hydrostatic pressure in the equations for densification. Since a powder compact can sinter under its own sintering pressure generated by the curvature at the pore surfaces, the total pressure, p, use in equations (3) and (4) is in fact the sum of the applied pressure, p_∞ and the intrinsic sintering pressure p_0:

$$p = p_\infty + p_0 = p_\infty + \frac{2\gamma}{\rho} \qquad (5)$$

Note that the sintering pressure depends on the surface energy of the pore surfaces, γ, and on the radius of curvature of the pores, r. Usually the magnitude of p_o lies in the range 1.0 MPa to 10.0 MPa. Thus p_o is negligible in comparison to the pressures commonly used in hot-isostatic-pressing (about 200 MPa). However, since powders can be sintered to nearly full density under their own sintering pressure, the need for such large superimposed pressures used in hot-isostatic-pressing can be questioned.

The functions $f(\rho)$ and $g(\rho)$ can be found in the detailed derivations given in references (6,9-12). As an example we give here the complete expression for final stage of densification by the diffusional mechansism[5]:

$$\dot{\rho} = 6.75 \frac{p\Omega}{kT} \frac{\delta D_b}{d^3} g(\rho) \qquad (6)$$

where

$$g(\rho) = \frac{1 - (1-\rho)^{2/3}}{3(1-\rho)^{2/3} - \{1 + (1-\rho)^{2/3}\} \ln(1-\rho)^{-3}} \qquad (7)$$

Here, Ω is the atomic volume, δD_b is the product of the grain boundary diffusion width and the grain boundary diffusion coefficient. Note that the expression $g(\rho)$ is numerically of order unity.

The experimental techniques for distinguishing between the dislocation and the diffusional mechanisms rely on studying the role of particle size and the stress on the densification rate. Later in this report we describe hot-pressing experiments which appear to span a transition from one to the other mechanism.

The Experimental Technique

The densification of powder compacts can be achieved through different paths. For example the powder compact may be hot-isostatically-pressed, or hot-pressed, or it may be extruded. In all cases full density is achieved, but the final shape of the dense object will be different as shown schematically in Fig. 1. The essential difference between the different processes lies in the amount of shear strain imparted to the powder compact during consolidation. The densification and the shear strain can be formally separated by carrying out sinterforging experiments under a uniaxial stress where the axial as well as the radial strains are measured, as illustrated in Fig. 2. The principal stresses and strains for such experiments are as follows:

$$[\sigma] = \begin{bmatrix} \sigma_z - p_o & 0 & 0 \\ 0 & -p_o & 0 \\ 0 & 0 & -p_o \end{bmatrix} \tag{8}$$

and

$$[\epsilon] = \begin{bmatrix} \epsilon_z & 0 & 0 \\ 0 & \epsilon_r & 0 \\ 0 & 0 & \epsilon_r \end{bmatrix} \tag{9}$$

Here σ_z is the uniaxial stress, p_o is the sintering pressure and ϵ_z and ϵ_r are the axial and radial strains respectively. Equations (8) and (9) can be used to define the densification strain, ϵ_a, and the shear or the effective strain, ϵ_e, as well as the pressure p, and the effective stress, σ_e:

$$p = -\frac{\sigma_z}{3} + p_o \tag{10}$$

$$\sigma_e = |\sigma_z| \tag{11}$$

$$\epsilon_a = |\epsilon_z + 2\epsilon_r| \tag{12}$$

and,

$$\epsilon_e = \frac{2}{3} |\epsilon_z - \epsilon_r| \tag{13}$$

Note that in the case of hot-isostatic-pressing $\varepsilon_z = \varepsilon_r$. For the case of hot pressing $\varepsilon_r = 0$, and we obtain the following simple relation between the shear and densification strain:

$$\epsilon_e = \frac{2}{3} \epsilon_a \tag{14}$$

In this report we shall describe the results for hot-pressing experiments. The results will be reported in terms of ε_a, that is the densification strain. We wish to caution the reader that hot-pressing also necessarily involves shear deformation (as defined by equation 14) and at this point it remains an open question whether the rate limiting step in our experiments was densification rate or shear deformation rate.

CHOOSING A MATERIAL FOR EXPERIMENTS

The choice of a suitable material for the experiments was based on the following criteria:

(i) The ability to vary the diffusion coefficients without affecting the dislocation yield stress. This would allow a separation of the diffusional and the dislocation mechanisms of densification.

(ii) Availability of a supplier who would prepare powders of desired composition and size distribution.

(iii) The material should have some relevance to a real life structural material for high temperature applications.

It was decided that a nickel-aluminum alloy would fit the above requirements. The diffusion coefficients and the dislocation yield strength for the alloy, for various nickel/aluminum ratio are shown in Figs. 3 and 4. The composition range $Ni_xAl_{(1-x)}$, where x lies in the range $0.64 < x < 0.52$ was chosen. In this range the diffusion coefficient is known to vary by more than a factor of 100, as shown by the data in Fig. 3. The nickel rich side was chosen because in this range the relative diffusivity of nickel and aluminum does not change, as also shown in Fig. 3[13]. The effect of the composition x on the dislocation yield stress is shown in Fig. 4 (courtesy Pratt and Whitney Aircraft). Note that the yield stress generally increases with x in the range we have chosen. this is also desirable since that would further increase the difference in the dislocation and the diffusion rates. Thus the diffusional rate of densification would be expected to accelerate with increasing x while the dislocation rate should decrease with higher x.

The compositions chosen for powder preparation are shown in the phase diagram shown in Fig. 5 as (1), (2) and (3). Note that (3) lies in the two phase region (δ and ε) while the other two compositions lie in the single phase (δ) region. The composition (3) was deformed at 1100°C which lies close to the phase boundary. This was chosen because of our experience that deformation near a phase boundary enhances ductility[14].

The exact theoretical densities of the three compositions were calculated using the lattice parameter data as a function of composition for the nickel aluminum alloys (Metals Handbook: Crystal Structure of Phases of Binary Alloy Systems; W.B. Pearson "Handbook of Lattice Spacings and Structure of Metals," vol. 1 and 2, Pergamon 1958 and 1967). That led to the following values:

	Theoretical Density
$Ni_{.52}Al_{.48}$	6.00 gm cm^{-3}
$Ni_{.58}Al_{.42}$	6.375 gm cm^{-3}
$Ni_{.64}Al_{.36}$	6.50 gm cm^{-3} (δ phase)
	7.31 (ε phase)

Powders for each composition were separated into four mesh sizes, the finest size being 500 mesh.

A description of the mechanical properties of the nickel-aluminum intermetallics can be found in reference 15.

The experiments reported in the next section were carried out on two compositions: $x = 0.52$ and $x = 0.64$. Powder mesh size of 500 was used.

EXPERIMENTAL RESULTS AND DISCUSSION

Experimental Method

Hot-pressing experiments were carried out with dies constructed from high purity graphite. The inside diameter of the die was 0.50". The inside was lined with graphoil of thickness 0.005". The die was filled with powder by tapping. The typical initial height of the powder was approximately 0.5". Hot-pressing was carried out inside a tungsten mesh furnace in a vacuum of 10^{-5} torr. The furnace was heated up from room temperature to the hot-pressing temperature (1050°C or 1100°C) linearly with time over a period of 45 mins. No load was applied to the specimen during this period. After the temperature was attained, a constant load was applied to the specimen and the change in the height of the specimen was measured by means of an LVDT. At the end of the experiment, the finish density and the height of the specimen were measured (at room temperature). This measurement of the height was used as the reference for adjusting the LVDT data.

Four specimens, two for each composition, one set corresponding to low applied stress and the other to high applied stress, were sectioned for metallographic analysis. The specimens were etched with Villela's reagant. The photographs shown later in this report were obtained in the scanning electron microscope in the normal (SEI) and in the back-scattered (BEI) mode.

Displacement vs. Time Curves

The change in the height of the specimen with time is plotted in Fig. 6 and 7 for various values of the applied stress. Since the diameter of the specimen remains constant during a hot-pressing experiment, the change in height is directly proportional to the change in density of the

specimen. The height has been normalized with respect to the height expected for a fully dense specimen. Thus $(L/L_0) = 1.0$ corresponds to full density. It follows that if V_0 is the volume of the dense material and ΔV is the porosity, then:

$$\rho = 1 - \frac{\Delta V_o}{V_o} = 2 - \frac{L}{L_o} \qquad (15)$$

where ρ is the relative density (actual density normalized with respect to the theoretical density). Note from equation (15) that ρ approaches unity as (L/L_0) approaches one.

The curves in Figs. 6 and 7 may be used to calculate the densification rate as a function of density and the applied load. The results can then be evaluated in terms of equations (3) and (4) to determine the pressure dependence of the densification rate. These results are described in the next section.

Densification Rate vs. Applied Stress

Densification rate curves for the (near) equimolar composition ($NiO_{.52}Al_{.48}$) are shown in Fig. 8, and for the nickel rich composition ($NiO_{.54}Al_{0.36}$) in Fig. 9. Each curve represents constant density.

The densification rate is found to decrease with increasing density. The slope of the curves also increases with increasing stress in the case of the equimolar composition. That is consistent with the increasing contribution from dislocations to the densification process at higher stress.

The most interesting result emerges when data from both compositions are plotted on the same graph, as shown in Fig. 10. Note here that the slope approaches unity for the nickel rich composition while it is equal to

3.0 for the equimolar case. A slope of unity implies diffusional densification, while the high value of the slope implies densification by dislocation mechanisms. This agrees with the expectation we had for the experiments that the higher diffusion coefficient of the nickel rich composition should favor the diffusional mechanism of densification.

Microstructures

The microstructures for the equimolar composition are shown in Figs. 1M, 2M and 3M. The first corresponds to densification carried out at 9.4 MPa and the others to 51.0 MPa. Note that full density is not achieved for this composition even at the high stress. The porosity in Fig. 1M is interconnected, so that grain size reflects the original particle size in the powder. The porosity has become isolated in Figs. 2M and 3M, which has allowed for some grain growth. In this case, as discussed just above, densification is believed to have taken place by the dislocation mechanism.

Microstructures for the nickel-rich composition are shown in Figs. 4M and 5M for the low stress experiments (8.5 MPa) and in Figs. 6M and 7M for the high stress experiments (18 MPa). Note that the grain growth is less for the low stress case, probably because the residual porosity has retarded grain boundary migration. At 18 MPa full density was obtained.

The unusual feature of the micrographs is the appearance of new grains at the grain boundaries when the powders were compacted at high stress. The grains/precipitates are most evident in the back-scattered micrographs shown in Figs. 3M and 7M. We are not certain at this point whether these grain boundary precipitates are a new phase or whether they are new grains of the parent phase. The appearance of the grains only at high applied stress suggests that these new grains represent the onset of dynamic recrystallization.

FUTURE WORK

The results presented in this report demonstrate that the change in stoichiometry and the applied stress can be used to distinguish between the diffusional and the dislocation mechanisms of densification. The hot-pressing experiments, however, are not the best way to study the densification behavior since the reaction stress applied by the die wall to the specimen is not known in such experiments. Future experiments, therefore, will be carried out in open die sinter-forging. The axial as well as the radial strains will be measured by the technique shown schematically in Fig. 2. Different processing paths will be used to apply increasing amounts of shear strain to the specimen during densification. The influence of this shear strain on (a) densification and (b) microstructure evolution, particularly dynamic recrystallization, will be examined in detail. The results will be interpreted in terms of theoretical models for densification.

REFERENCES

1. J.S. Benjamin and T.E. Volin, Metall. Trans. A, vol. 5A, p. 1929 (1974).
2. "Fundamentals of Compaction for Rapidly Quenched Pre-Alloyed Metal Powders", G.J. Hilderman, D.J. Lege, and A.K. Vasudevan, Report AFWAL-TR-82-4156, ALCOA, Alcoa Center, PA, Oct. 1982.
3. "Elevated Temperature Aluminum Alloy Development", R.E. Sanders, Jr. and G.J. Hilderman, ALCOA, Alcoa Center, PA, September 1981.
4. D.S. Wilkinson and M.F. Ashby, Acta Metall., vol. 23, p. 1277 (1975).
5. "Mechanism Mapping of Sintering under an Applied Pressure", D.S. Wilkinson and M.F. Ashby, Science of Sintering, vol. 10, pp. 67-76 (1978).
6. "Practical Applications of Hot-Isostatic Pressing Diagrams: Four Case Studies", F. Arzt, M.F. Ashby, and K.E. Easterling, Metall. Trans., vol. 14A, p. 211 (1983).
7. H.J. Frost and M.F. Ashby, Deformation Mechanism Maps, Pergamon Press, (1982).
8. A.K. Ghosh, Deformation of Polycrystals - Mechanisms and Microstructures, Proc. 2nd RISO Int. Symp. Metall. Mater. Sci., eds., N. Hansen, et al., p. 277 (1981).
9. "Void Growth and Collapse in Viscous Solids", Mechanics of Solids, eds., H.G. Hopkins and M.J. Sewell, Pergamon Press, p. 13 (1982).
10. "The Strain-Hardening Hollow Sphere Compaction Model Applied to Aluminum", International J. Powder Metall. & Powder Tech., vol. 10, p. 131 (1974).
11. "Powder Consolidation", A. Lawley, Advances in Powder Technology, ed., G.Y. Chin, ASM, Metals Park, OH, p. 75 (1982).
12. "Effects of Porosity in Materials Processing", H.A. Kuhn, The Effects of Voids on Material Deformation, eds., S.C. Cowin and M.M. Carroll, ASME, NY, p. 171 (1977).
13. S. Shankar and L.L. Siegle, Metall. Trans. A, vol. 9A, p. 1467 (1978).

14. "Superplastic Deformation in Fine-Grained MgO, $2Al_2O_3$ Spinel", P.C. Panda and R. Raj, J. Amer. Ceram. Soc., vol. 68[10], pp. 522-529 (1985).

15. "Investigations of NiAl and Ni_3Al", E.M. Grala, Mechanical Properties of Intermatallic Compounds, ed., J.H. Westbrook, John Wiley and Sons, Inc., NY (1960).

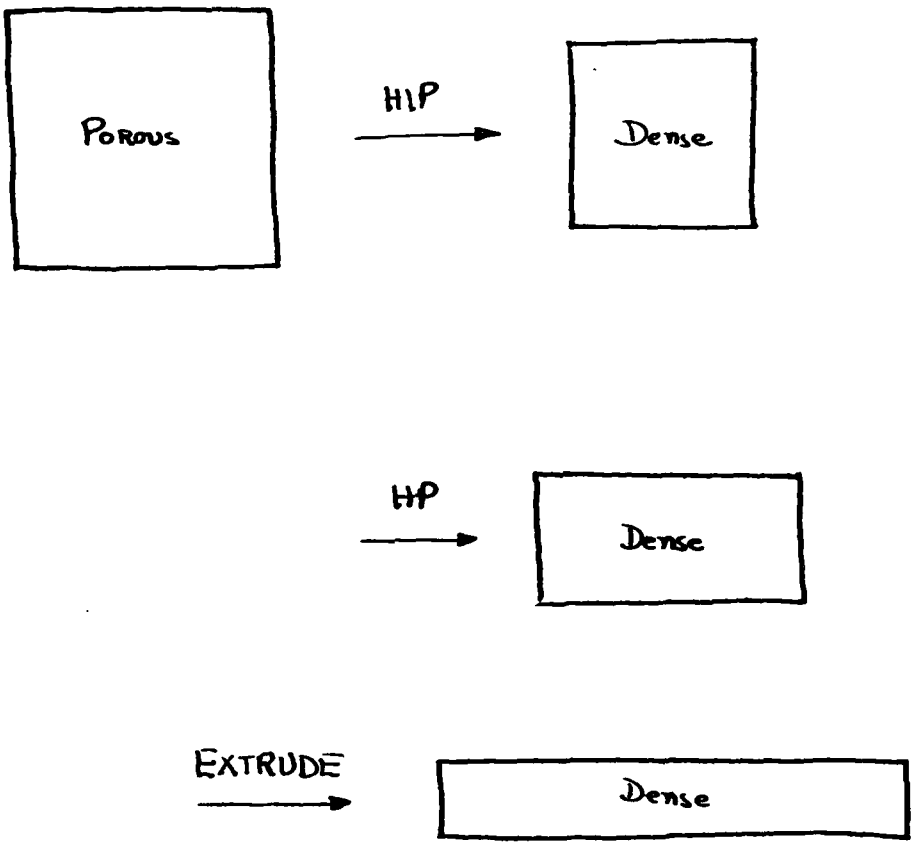

1. Hot-isostatic-pressing or sintering produce only a change in volume without a change in shape, while hot-pressing and extrusion cause both densification and a change in shape. Thus, the latter two apply a combination of densification and shear strain to the powder compact.

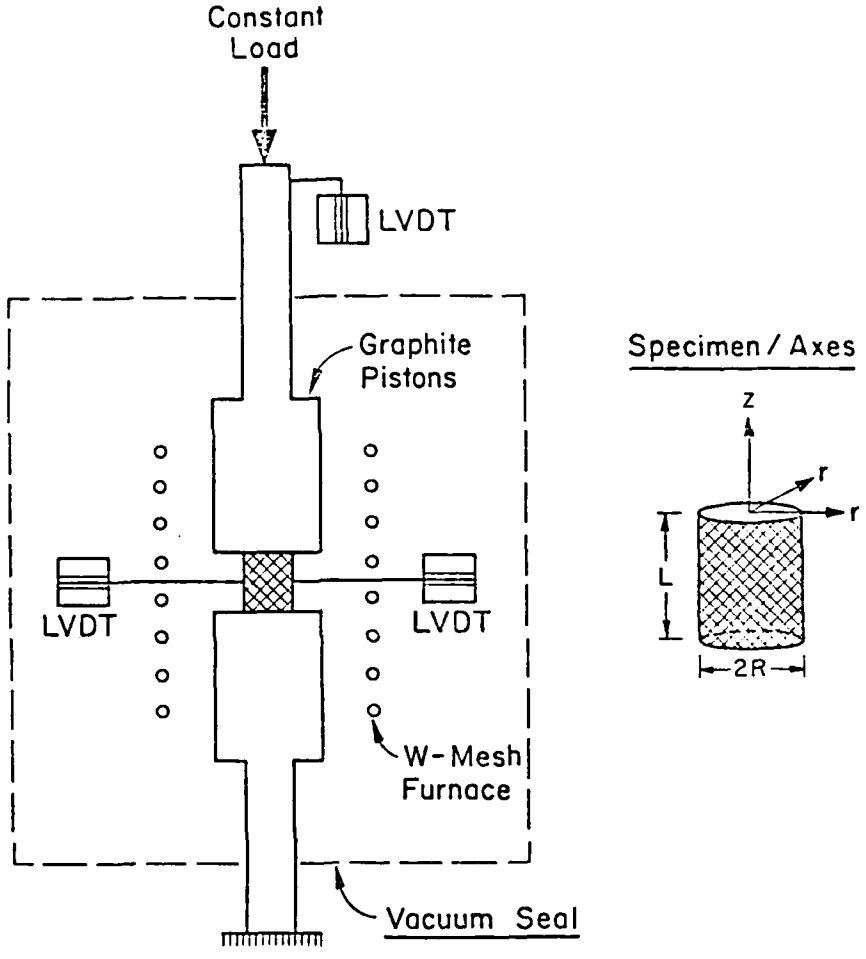

2. A schematic of the experimental set-up which will be used to measure the combined densification and shear deformation behavior of the powder compacts.

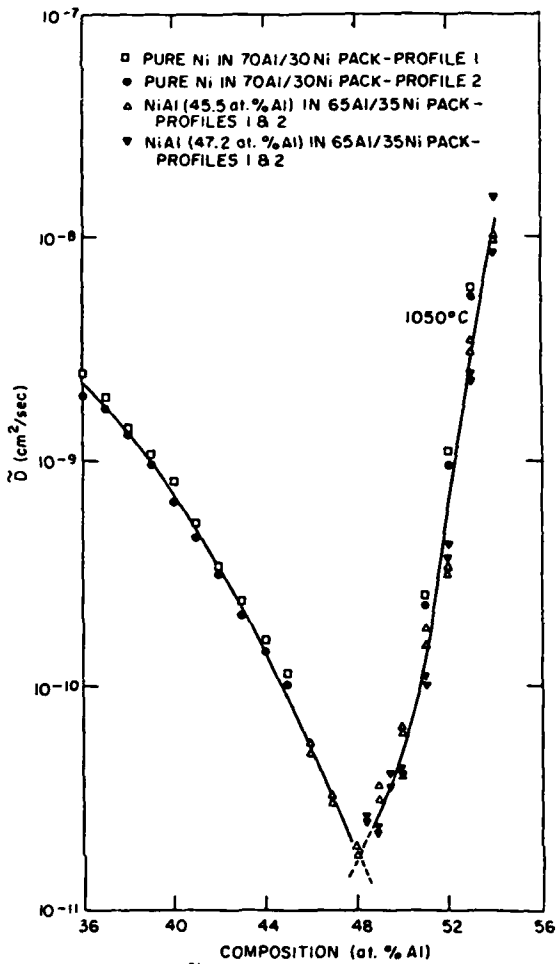

Variation of $\tilde{D}$ with composition in NiAl (δ)—1050°C.

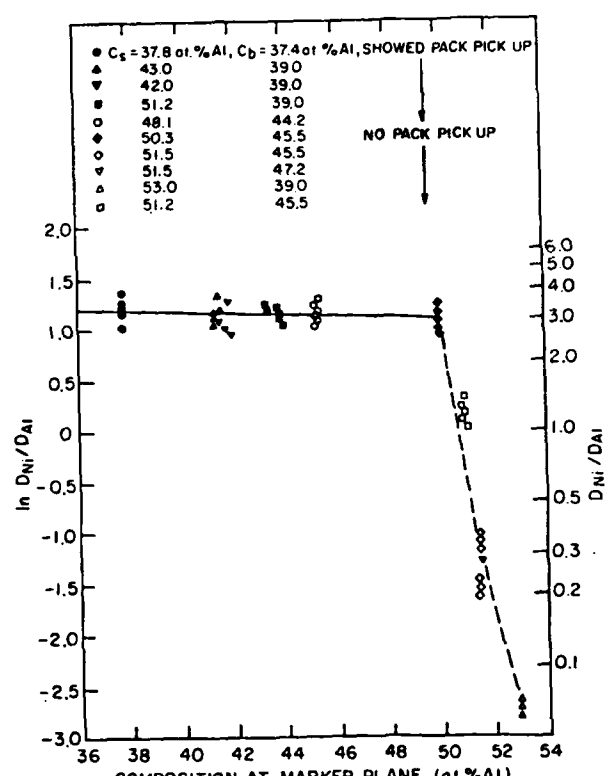

Variation of D_{Ni}/D_{Al} with composition in NiAl (δ) at 1100°C. C_s = Composition at surface ($\pm$0.2 at. pct Al); C_b = Composition of base alloy used ($\pm$0.1 at. pct Al).

3. Intrinsic diffusion data for nickel-aluminum as a function of stoichiometry (Ref. 13).

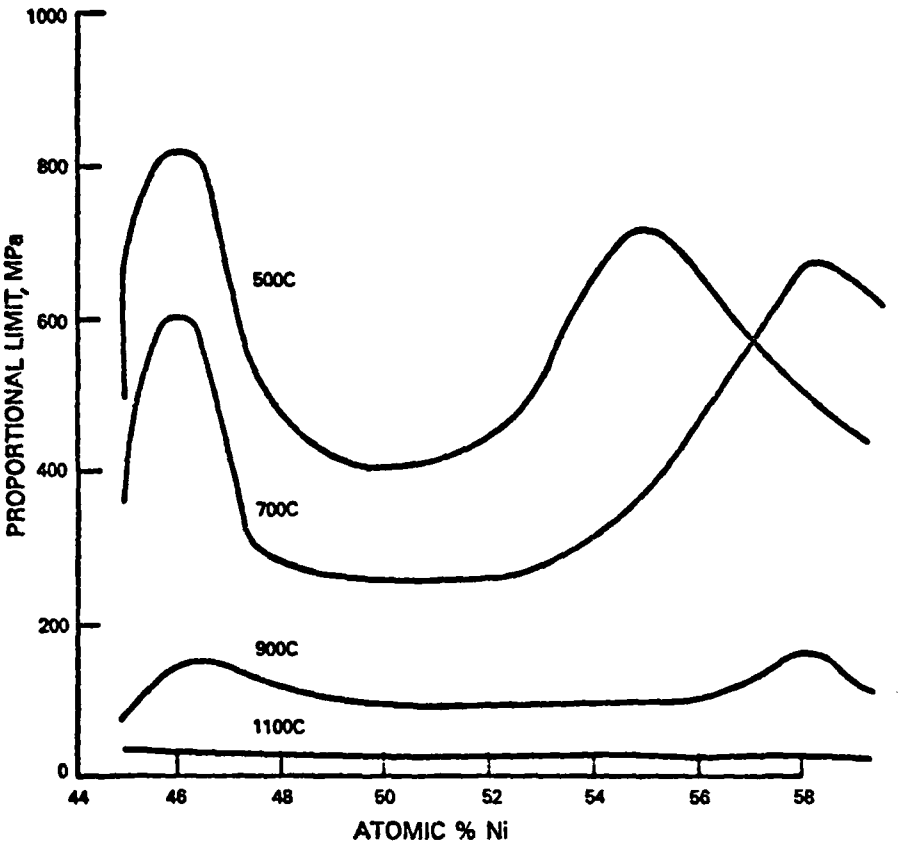

4. Yield stress for nickel-aluminum as a function of composition and temperature (courtesy Pratt and Whitney Aircraft).

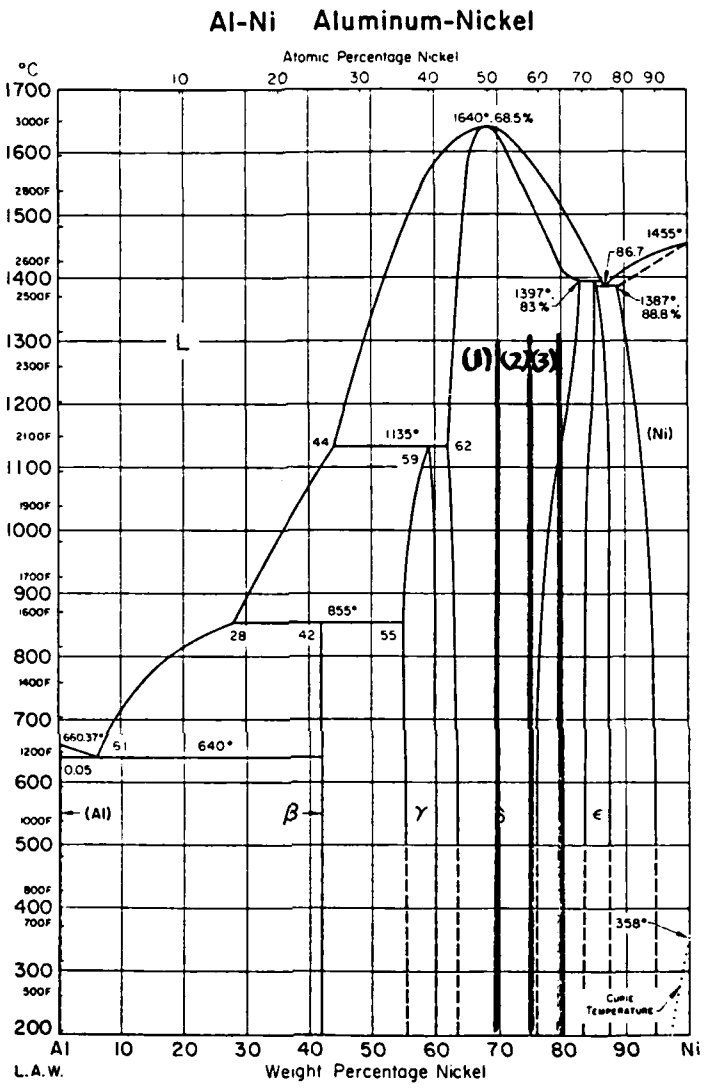

5. The three compositions of nickel-aluminum chosen for experiments.

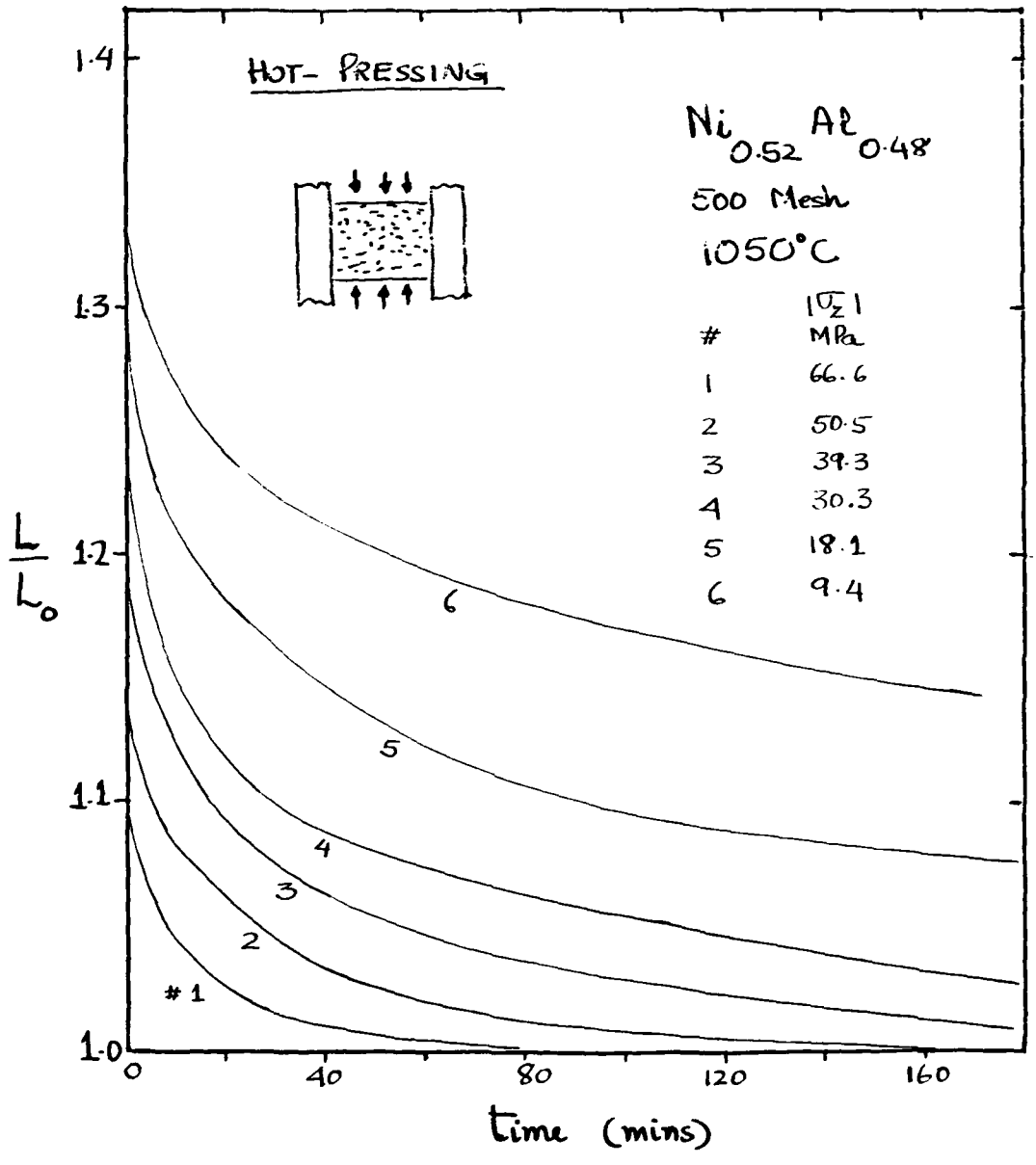

6. Displacement/time curves for the (near) equi-molar composition at various values of the applied stress in hot pressing experiments. Each curve represents a new experiment.

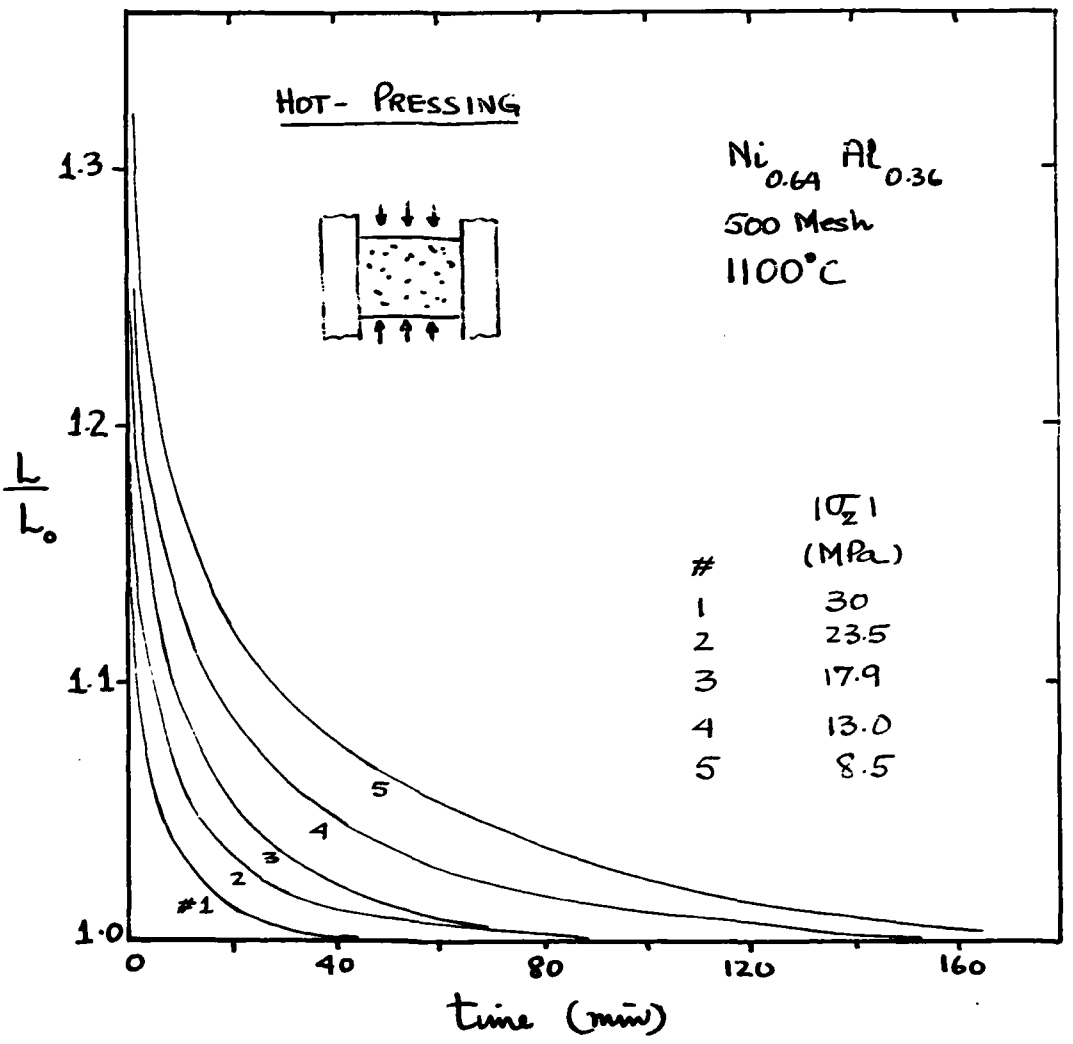

7. Displacement/time curves for the nickel rich composition at various applied loads. Each curve represents a new hot-pressing experiment.

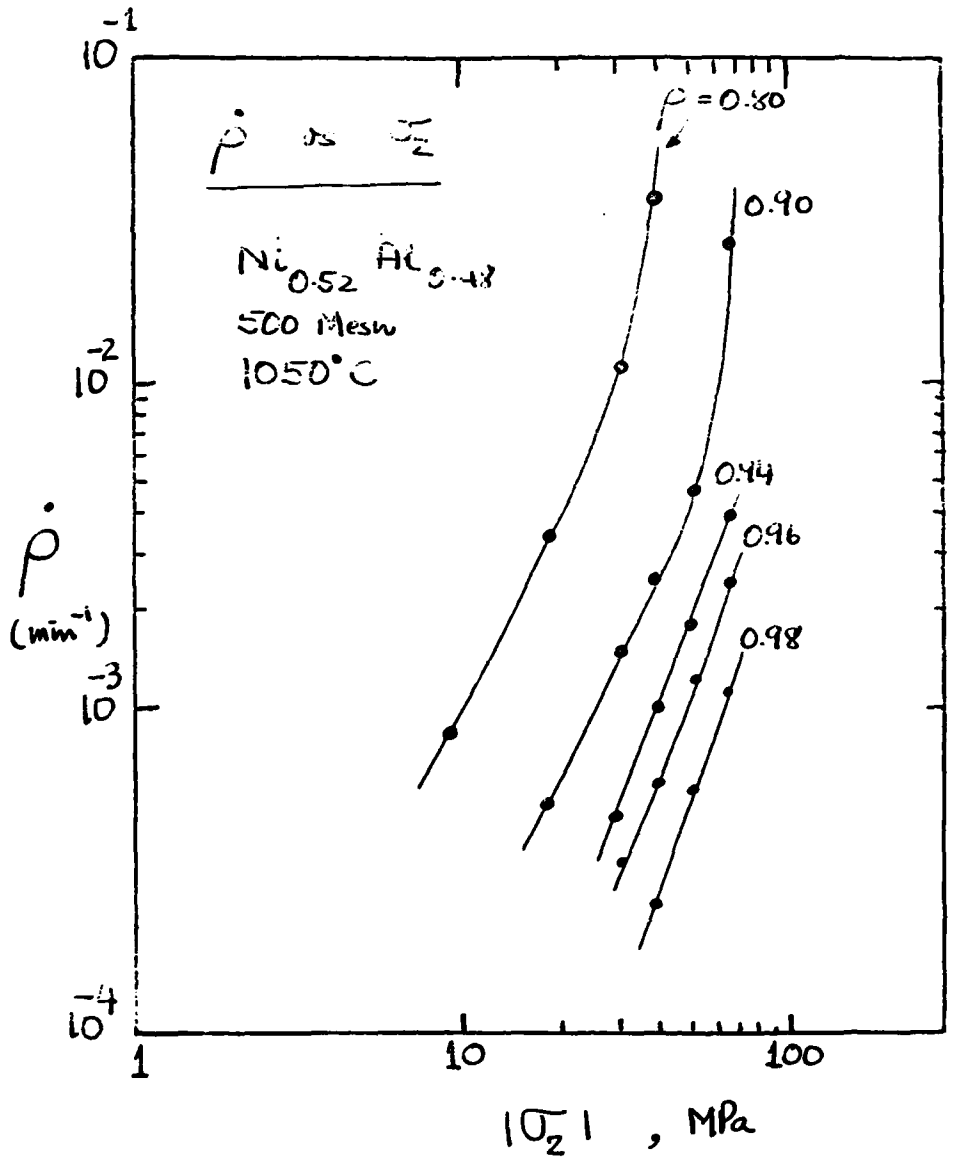

8. Densification rate vs. stress curves obtained from the data in Fig. 6.

Copy available to DTIC does not permit fully legible reproduction

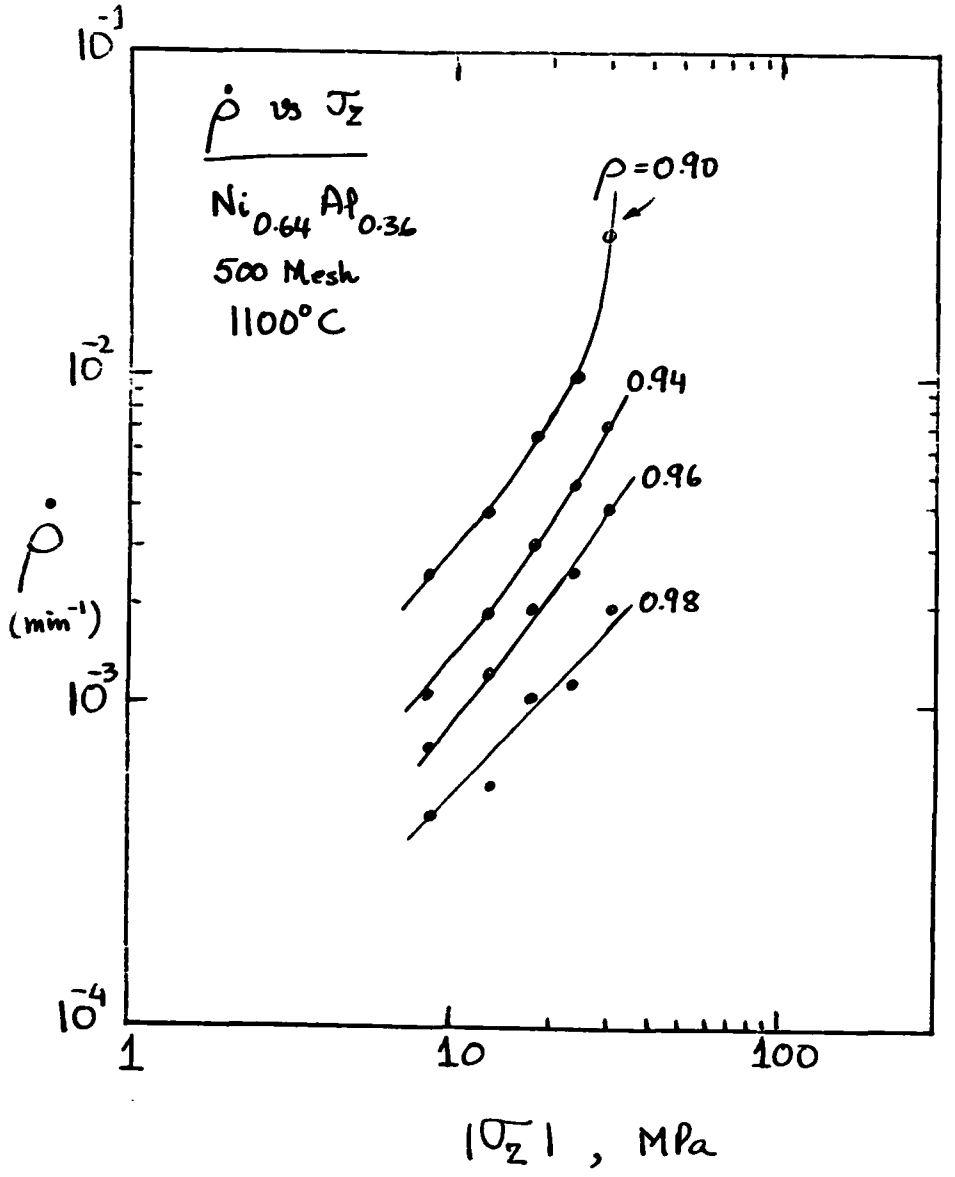

9. Densification rate vs. stress curves obtained from the data in Fig. 7.

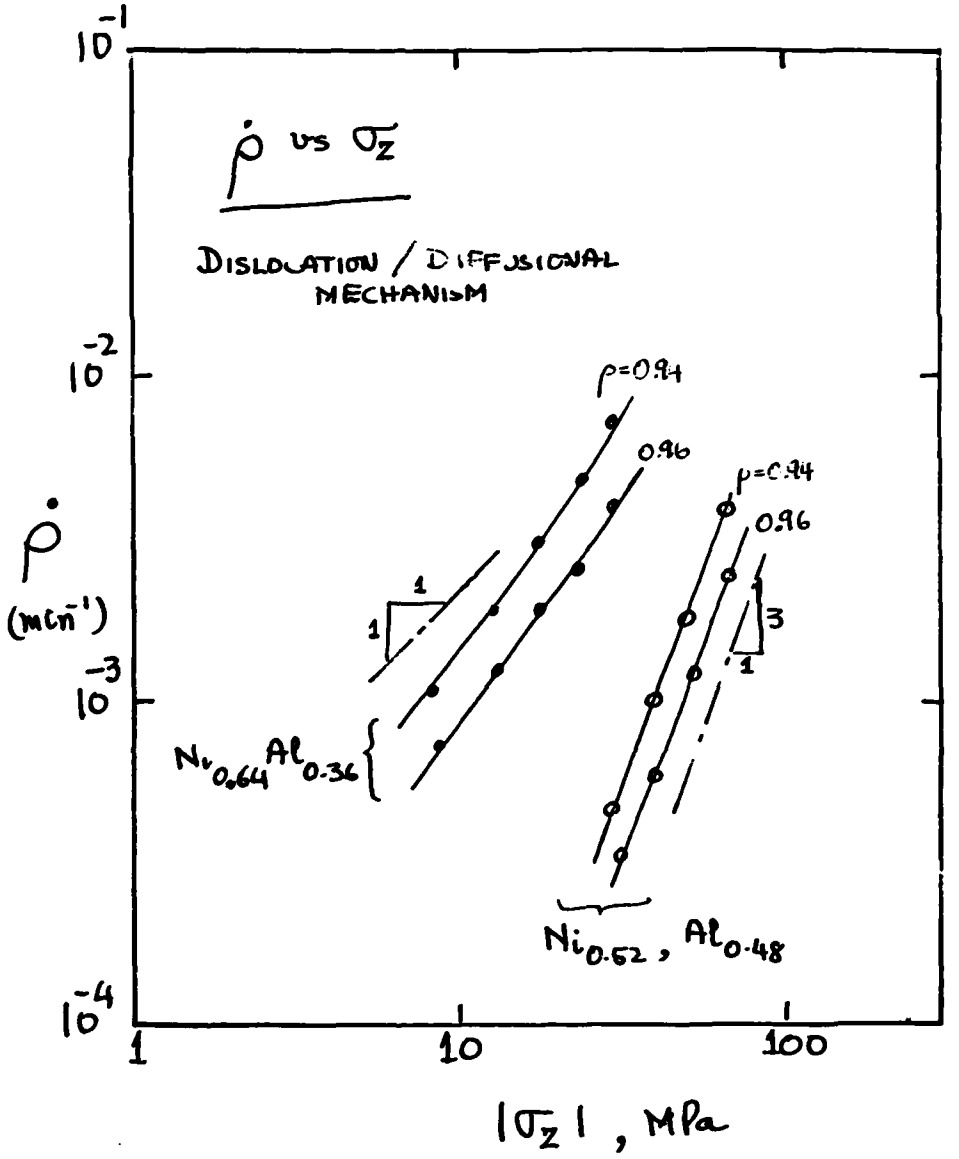

10. A comparison between the densification rate curves for the equi-molar and the nickel rich compositions. The higher slope of the curves for the equi-molar case implies a dislocation mechanism of densification, while the near unity slope for the nickel-rich composition implies diffusional densification.

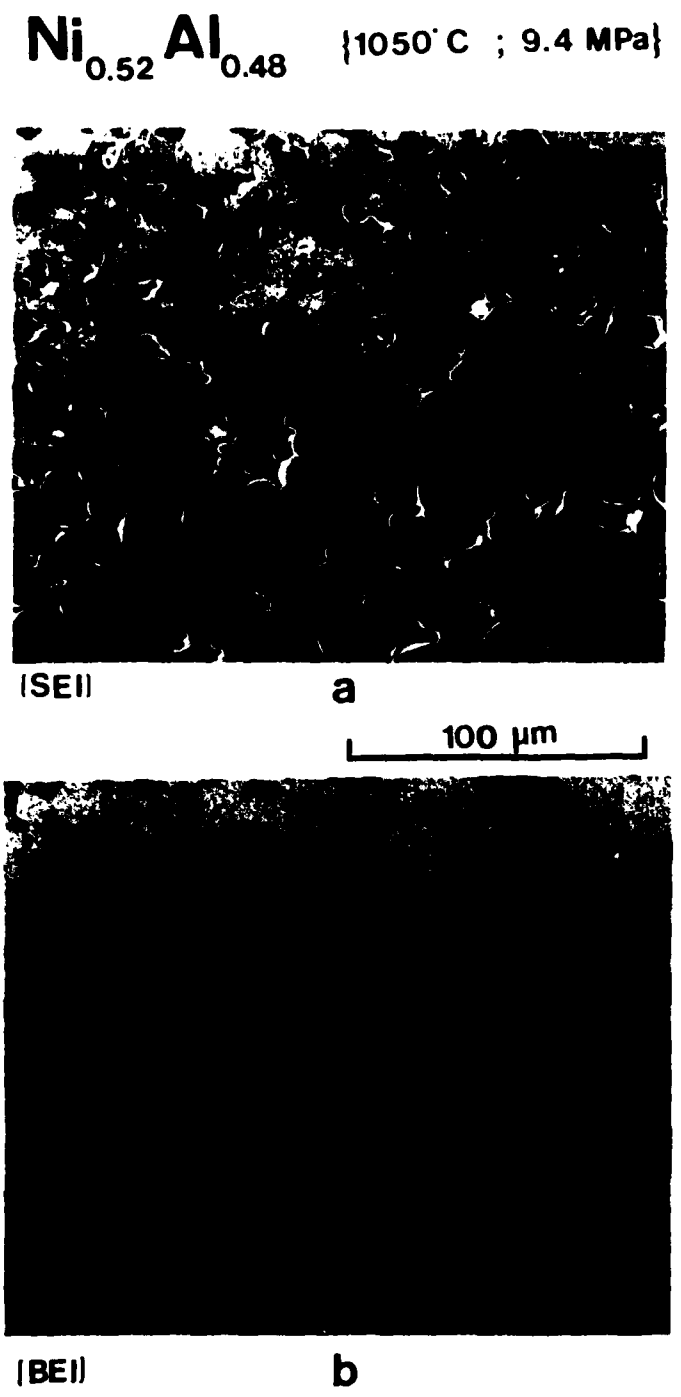

Figure 1 Near-equimolar Ni/Al hot-pressed at low stress. Final density is approximately 87%. At this stage the porosity is probably interconnected. (NA1-1)

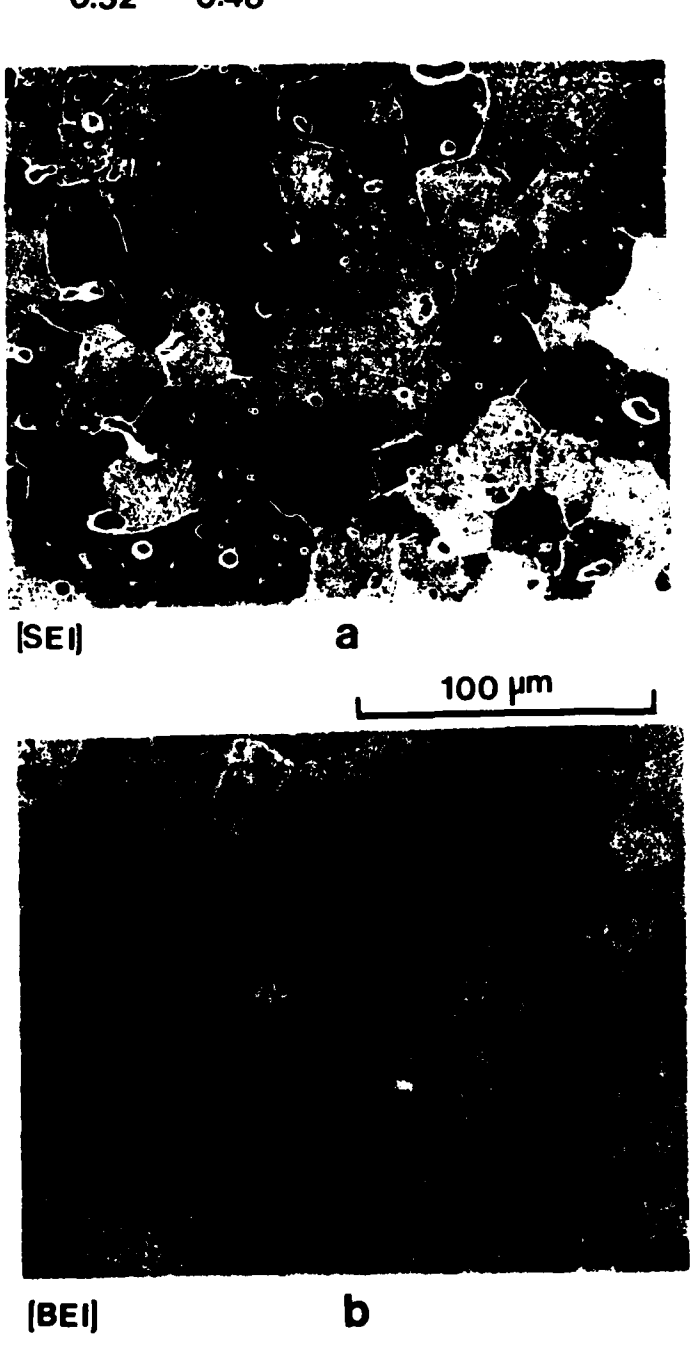

Figure 2 Near-equimolar Ni/Al hot-pressed at high stress. Finish density is approximately 93%. Note the appearance of a second phase at the grain-boundaries.(NA1-3)

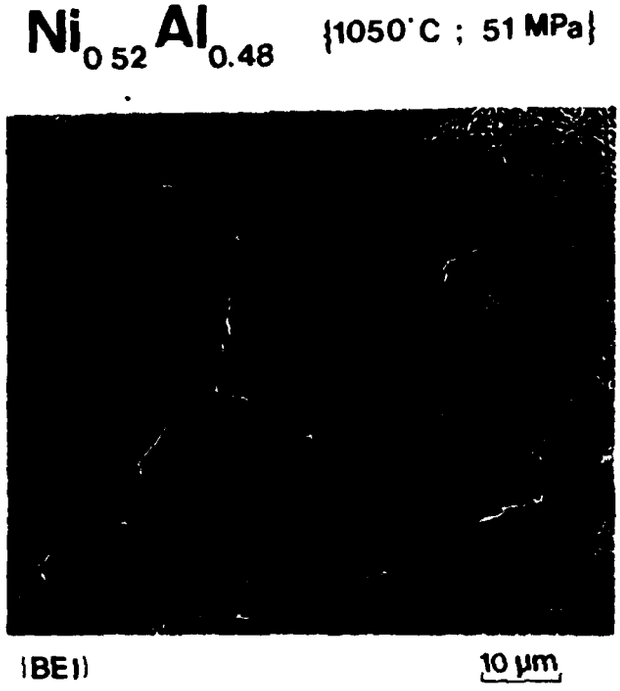

Figure 3 A magnification back-scattered scanning electron micrograph showing the precipitation of a second phase at grain boundaries during deformation. (NA1-3)

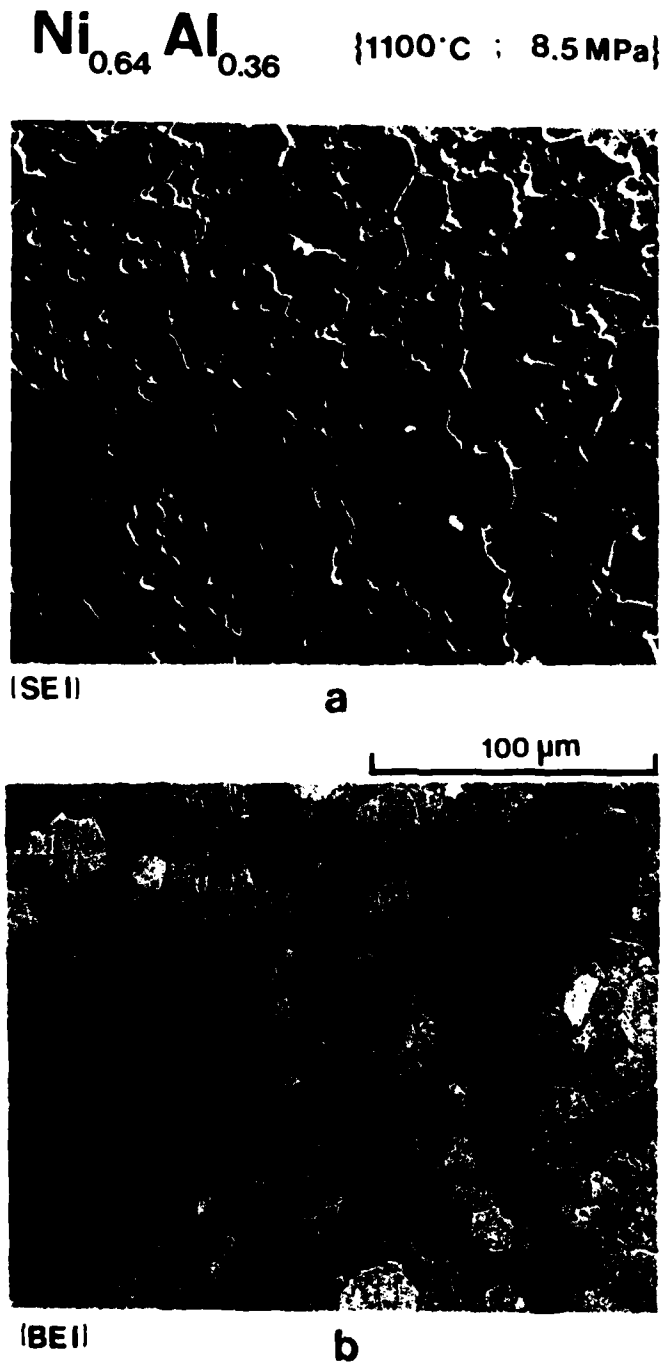

Figure 4 Nickel-rich Ni/Al hot pressed at low stress. Note the fine grain size and the higher density as compared to the equimolar composition shown in Fig. 1. (Spec. NA3-1)

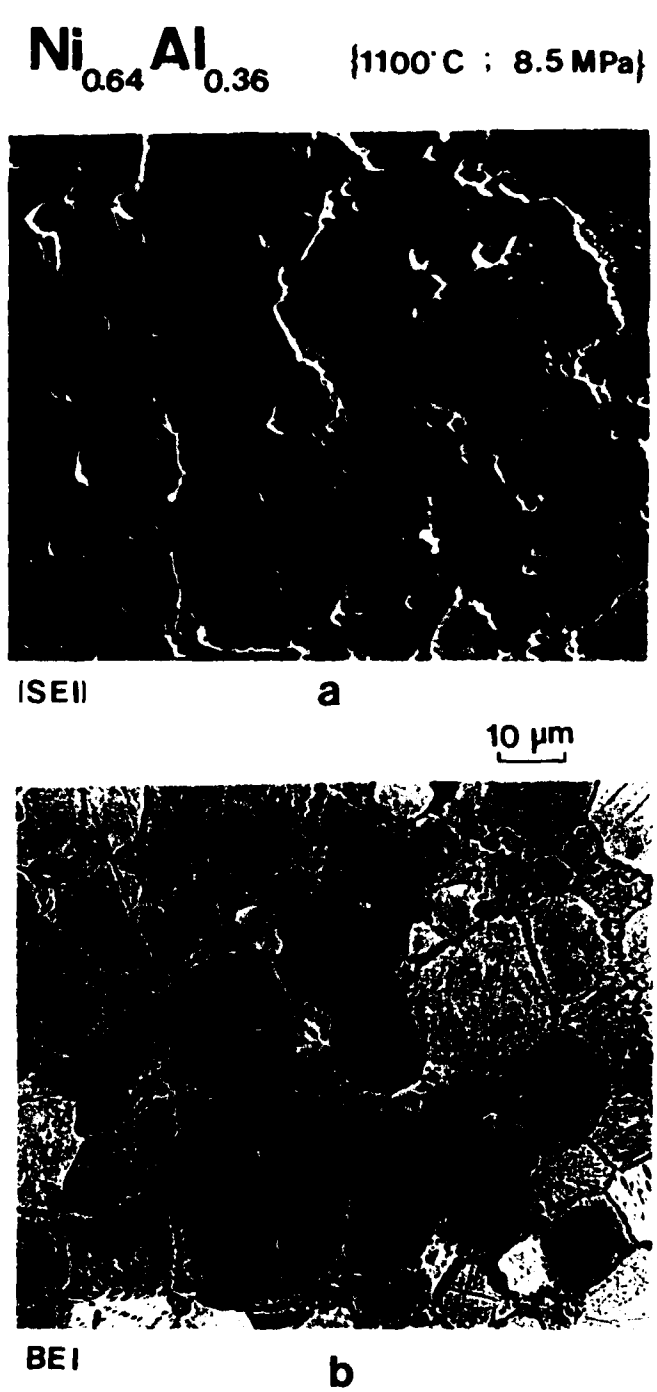

Figure 5 Same as Fig. 4 viewed in higher magnification. Note that compared to the high stress case shown in Figs. 6 and 7, this case does not show a second phase at grain boundaries. (Spec. #NA3-1)

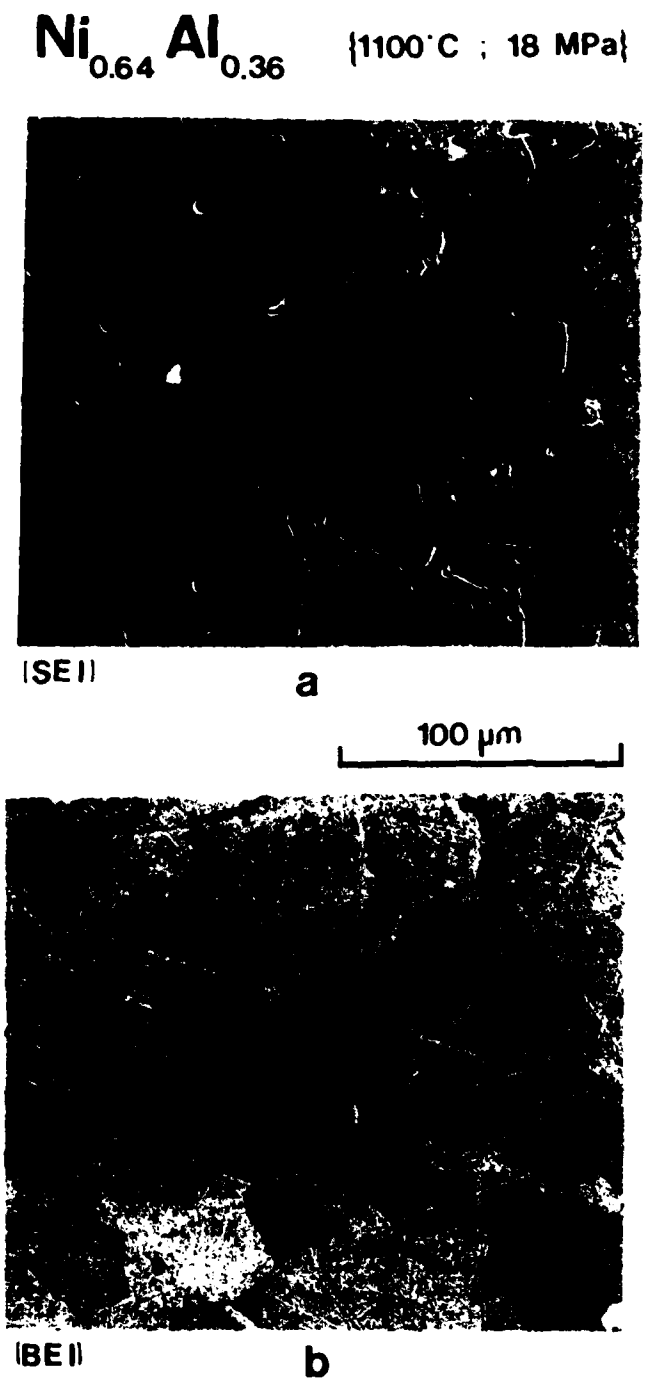

Figure 6 Nickel-rich Ni/Al hot-pressed at high stress. Note the larger grain size in comparison to the equimolar Ni/Al shown in Fig. 2. (Spec. #NA3-2)

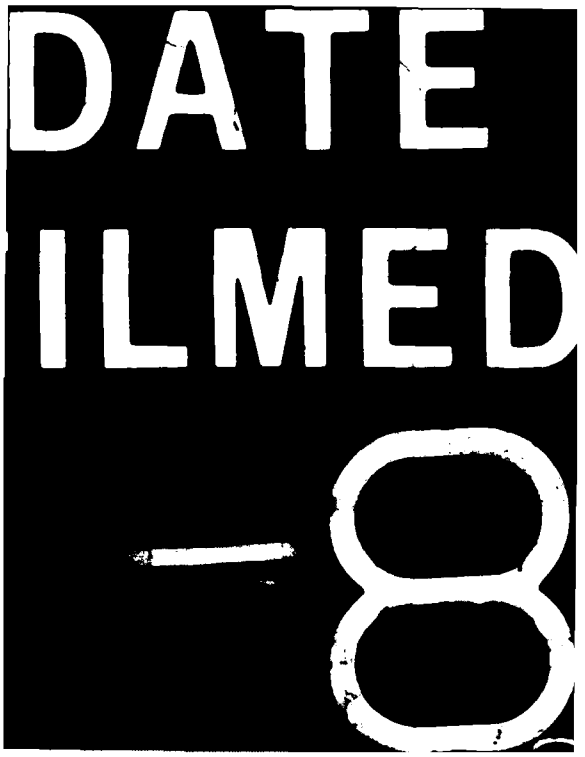
DATE
ILMED
-8